

Electronic Supplementary Material

**Controlled synthesis of highly reactive (111) facets exposed TiO₂
nanocuboids decorated nanotubes and nanowires hybrid structure
with enhanced photoelectrochemical properties**

Dong Ding, Bo Zhou, Shuang Feng, Li Liu, Fei Feng, Runa A, Pengyu Su, Jun Wang,

*Wuyou Fu and Haibin Yang**

State Key Laboratory of Superhard Materials, Jilin University, Changchun 130012,

PR China. E-mail: yanghb@jlu.edu.cn

Preparation of original TiO₂WTs photoelectrode: All chemicals used were of the highest purity available and used as received without further purification. Deionized water was used in all cases. TiO₂WTs photoelectrode was prepared by electrochemical anodization of a Ti foil (4 cm×3 cm, 0.4 mm thick, 99.9% purity). Ti foil was cleaned and dried before anodization. Electrochemical anodization was carried out on a direct current (dc) stabilized voltage and current power supply (WYJ60V3A, Pingguo instrumentation Co. Ltd. China) with a constant voltage of 40 V at room temperature for 1 h. Ti foil was used as an anode, with a graphite plate as cathode in an ethylene glycol electrolyte solution containing 0.3wt% NH₄F, 5.0 vol% deionized H₂O. Then, the as-prepared photoelectrode was thoroughly washed with ethanol and then DI water, and then annealed in the air at 450 °C for 2 h.

Preparation of TiO₂ PWTs photoelectrodes: For a typical synthesis, TiO₂WTs photoelectrodes was immersed into aqueous solution containing 25mM TiCl₄ at 70 °C for 20 min. Then, the treated photoelectrode was washed with DI water and annealed in the air at 450 °C for 1h.

Preparation of TiO₂ FWTs photoelectrodes: For a typical synthesis, TiO₂WTs photoelectrodes was immersed into aqueous solution containing 25mM TiCl₄ and 5.2 mM NH₃·H₂O at 70 °C for 20 min. Then, the treated photoelectrode was washed with DI water and annealed in the air at 450 °C for 1h.

Prepare of TiO₂ C₀₀₁WTs photoelectrodes: For a typical synthesis, TiO₂WTs photoelectrodes was immersed into aqueous solution containing 25mM TiCl₄ and 15.6 mM NaF at 70 °C for 20 min. Then, the treated photoelectrode was washed with DI water and annealed in the air at 450 °C for 1h.

In order to obtain a fair comparison, before characterization, also original TiO₂WTs photoelectrode was secondly annealed at 450 °C in air for 1h.

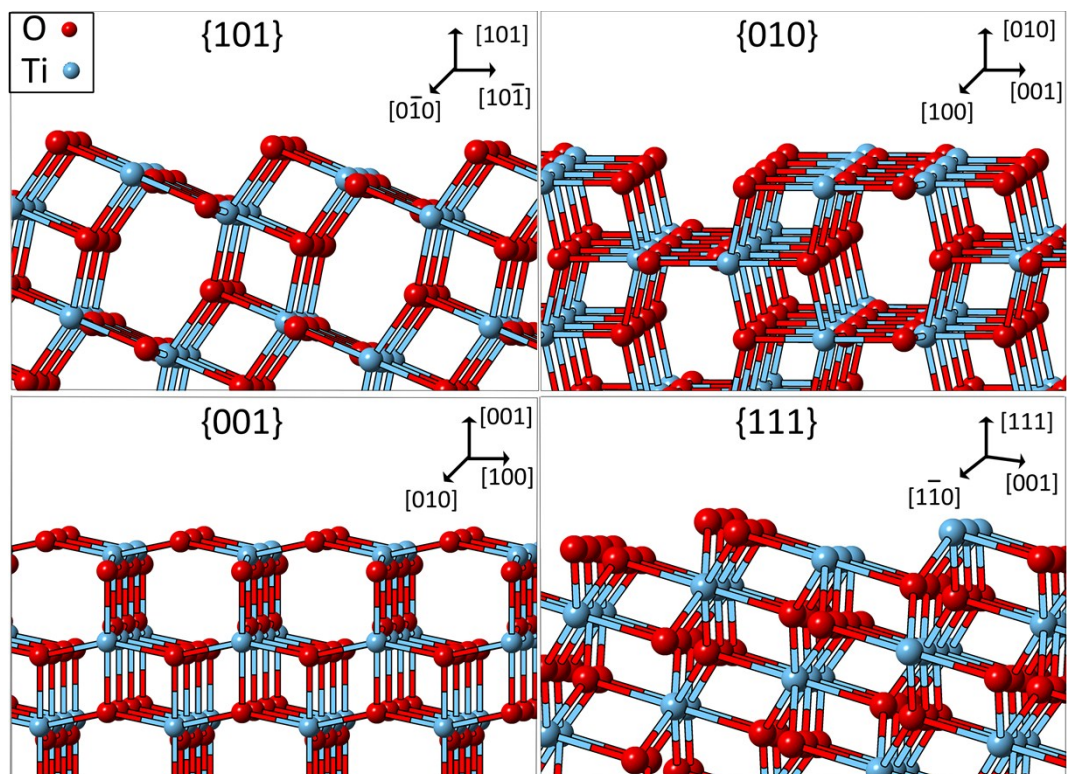


Fig.S1 Surface structures of {101}, {010}, {001} and {111} facets of anatase TiO_2 .¹

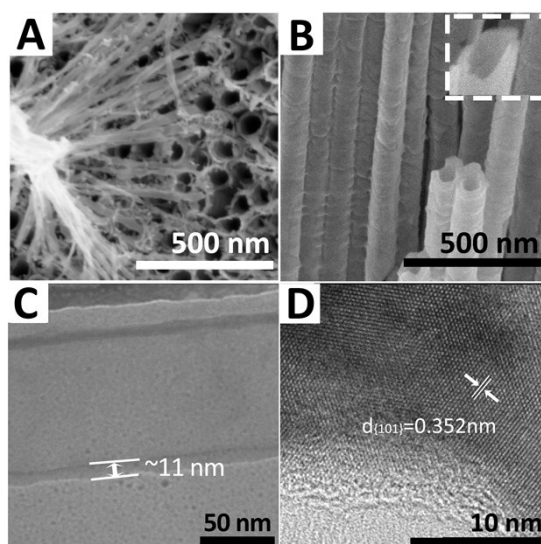


Fig.S2 SEM images (top and side views) of TiO₂WTs (A, B), TEM and HR-TEM images (C, D) of TiO₂WTs.

SEM and TEM images of original TiO₂ WT are shown in Fig.S2, Fig.S2 A is the top view of TiO₂WTs, it is shown that nanowires are loosely arranged on the top of the nanotubes and some pores are exposed. Nanotubes are formed through anodization process and nanowires are formed at the top sites of nanotubes with the effect of chemical etching.² Fig. S2B is the side view of TiO₂ WT, which shows that nanotubes are smooth with average pore diameter of ~75 nm. Fig.S2C is TEM image of TiO₂ nanotube. The tube is relatively smooth, and average thickness of tube wall is ~11 nm. Fig.S2D is HR-TEM image of TiO₂ nanotube. The lattice fringes with interplanar spacing (lattice distance) $d_{\{101\}} = 0.352$ nm in Fig.S2D is consistent with the anatase phase of TiO₂ [JCPDS no.71-1166].

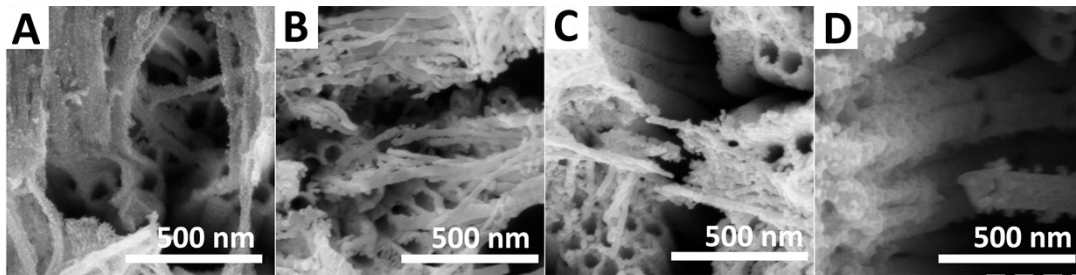


Fig.S3 SEM images (top views) of TiO_2PWTs (A), TiO_2FWTs (B), $\text{TiO}_2\text{C}_{001}\text{WTs}$ (C) and $\text{TiO}_2\text{C}_{111}\text{WTs}$ (D). These samples retain their original WT structure after treatments.

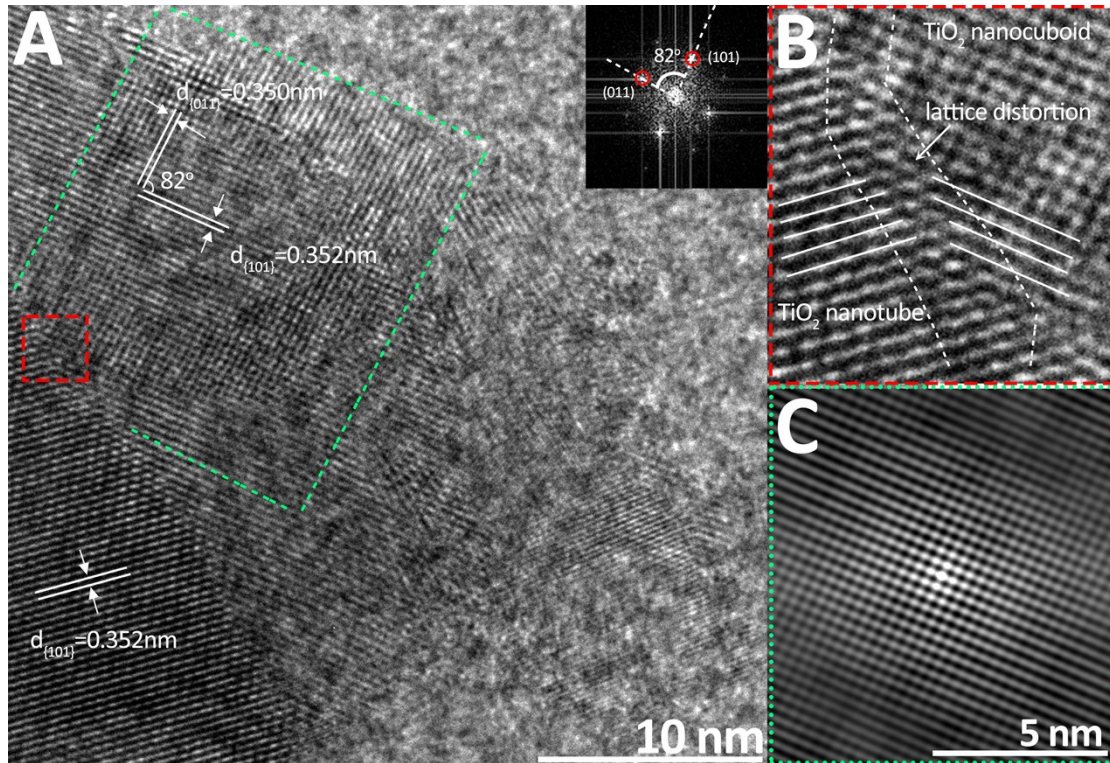


Fig.S4 HR-TEM image of $\text{TiO}_2\text{C}_{111}$ WTs (A) and enlarged HR-TEM images of interface for TiO_2 nanotube and nanocuboid (B). Inset in A is fast-Fourier transform (FFT) pattern of the cuboid.

Inset in Fig.S4A is fast-Fourier transform (FFT) pattern of the cuboid, which refers to $\{101\}$ facets and $\{011\}$ facets, respectively. The lattice spacings of 0.352 nm and 0.350 nm are lying with an angle of 82° , matching the spacing between $\{101\}$ and $\{011\}$ planes of anatase TiO_2 with $[111]$ zone axis, which confirms the top and bottom exposed crystal plane of the cuboid is $\{111\}$ facet.

The growth interfaces of nanocuboid and nanotube were observed in Fig.S4A, the joint part is magnified and shown in Fig.S4B, while the planes of nanocuboid are connected to the $\{101\}$ planes of TiO_2 nanotube (lattice fringes in the bottom left) via lattice distortion area, revealing the nanocuboid is grown on the nanotube. Fig.S4C is correlation of the area in green dash rectangle, the pattern indicates a single crystalline

structure. The growth interfaces of nanocuboid and nanotube result in more charge transfer channels, which can enhance the electronic injection.

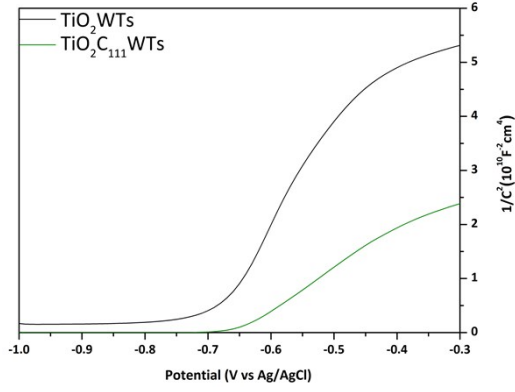


Fig.S5 Mott-Schottky plots of TiO₂ WTs and TiO₂C₁₁₁ WTs photoelectrodes.

As shown in Fig.S5, Mott-Schottky plots were collected at a frequency of 5 kHz for the TiO₂ WTs and TiO₂C₁₁₁ WTs photoelectrodes. The positive slopes in Mott-Schottky plots indicate both TiO₂ WTs and TiO₂C₁₁₁ WTs are n-type semiconductors.³ The major difference between these two photoelectrodes is that TiO₂C₁₁₁ WTs has a smaller slope in a Mott-Schottky plot compared to the TiO₂ WTs, suggesting an increase of donor densities. Charge carrier densities of TiO₂ WTs and TiO₂C₁₁₁ WTs were calculated from the slopes of the Mott-Schottky plots *via* the expression:⁴

$$N_d = (2/e_o\varepsilon_o\varepsilon)[d(1/C^2)/dV]^{-1}$$

where N_d presents the donor density, e_o is the elemental charge, ε_o is the vacuum permittivity, ε is the dielectric constant of TiO₂ ($\varepsilon=170$),⁴ C is the space charge capacitance in the semiconductor, and V is the applied bias at the electrode. Charge carrier densities of TiO₂ WTs and TiO₂C₁₁₁ WTs were calculated to be $0.4312 \times 10^{21} \text{ cm}^{-3}$ and $1.042 \times 10^{21} \text{ cm}^{-3}$, respectively. The increased donor density of TiO₂C₁₁₁ WTs improves the charge transport, which benefits PEC performance enhancement.

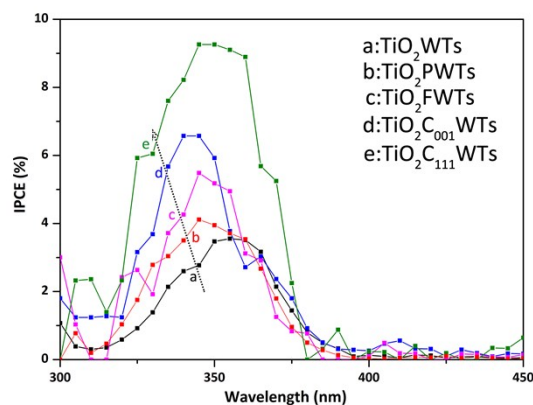


Fig.S6 Incident photon-to-current conversion efficiency (IPCE) of TiO₂WTs (a), TiO₂PWTs (b), TiO₂FWTs (c), TiO₂C₀₀₁WTs (d) and TiO₂C₁₁₁WTs (e) electrodes.

IPCE was measured using an action spectrum measurement setup (PEC-S20, Peccell Ltd.). Before the measurement, the samples were sealed in sandwich structures with a 60 μ m spacer by using Pt as the counter electrode. The electrolyte (0.25 M Na₂S · 9H₂O, 0.35 M Na₂SO₃ and 0.1 M KCl aqueous solution) was injected between the two electrodes. Light was illuminated from the counter electrode side. Fig.S6 shows that TiO₂C₁₁₁WTs electrode presents the best IPCE of round 9.3 % across the absorption ranges, which is higher than other electrodes (highest IPCE is ~6.5 % for TiO₂C₀₀₁WTs > ~5.5 % for TiO₂FWTs > ~4.1 % for TiO₂PWTs > ~3.5 % for TiO₂WTs), indicating that electron-hole pairs are separated more efficiently in TiO₂C₁₁₁WTs electrode and resulting in an enhanced PEC performance.

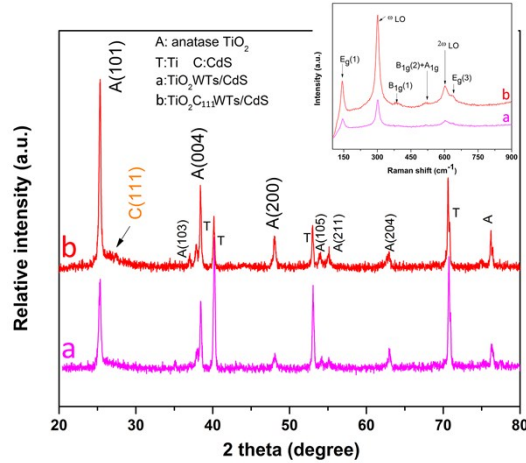


Fig.S7 XRD patterns and Raman spectra of CdS/TiO₂WTs (a) and CdS/TiO₂ C₁₁₁WTs (b) photoelectrodes.

Fig.S7 shows XRD patterns of TiO₂ WTs and TiO₂ C₁₁₁WTs sensitized by CdS (denoted as CdS/TiO₂ WTs and CdS/TiO₂ C₁₁₁WTs, respectively). XRD patterns for these two samples exhibit a new small peak at 2-theta of 27°, this new peak can be indexed to the {111} planes of the cubic-phase CdS [JCPDS no. 80-0019]. Inset of Fig.S7 is the Raman spectra, after sensitized by CdS, two additional peaks were detected, the peak at 305 cm⁻¹ and 605 cm⁻¹ are ascribed to the longitudinal optical (1LO) phonon mode of CdS and its overtone (2LO) mode, respectively.⁵ The relatively high intensity peaks of CdS for CdS/TiO₂ C₁₁₁WTs may correspond to the relatively big amount of CdS. This may due to more high-reactive (111) facets of TiO₂ C₁₁₁WTs, which offer the oxygen vacancies and would allow more Cd²⁺ adsorption on the surface of TiO₂ during SILAR process, and thus increase the formation of CdS-TiO₂ heterojunction. The enhanced CdS amount is one of the major reasons for the photoelectric performance enhancement, which improves the number of CdS/TiO₂ heterojunctions, and correspondingly increases the photocurrent density.

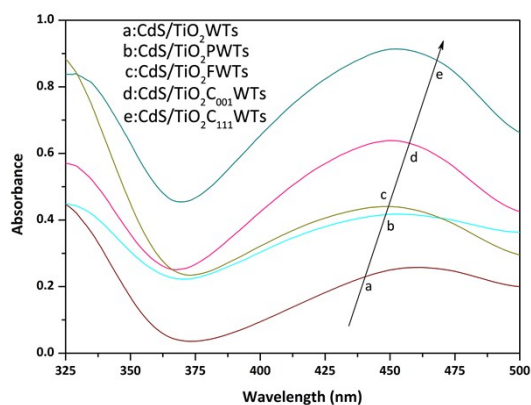


Fig.S8 UV-vis absorption spectra of CdS sensitized TiO₂ WTs/TiO₂ PWTs/TiO₂ FWTs/TiO₂ C₀₀₁WTs and TiO₂ C₁₁₁WTs photoelectrodes.

As shown in Fig.S8, UV-vis absorption spectra of CdS QDs sensitized TiO₂WTs/TiO₂PWTs/TiO₂FWTs/TiO₂C₀₀₁WTs and TiO₂C₁₁₁WTs photoelectrodes exhibit broad absorption bands from 370 to 500 nm. This variation indicates that the deposition of CdS QDs has significantly extended the photoresponse of these samples into the visible light region. Furthermore, the absorption intensity for CdS/TiO₂ C₁₁₁WTs is stronger than other photoelectrodes, which indicates the increased amount of CdS QDs for CdS/TiO₂C₁₁₁WTs.

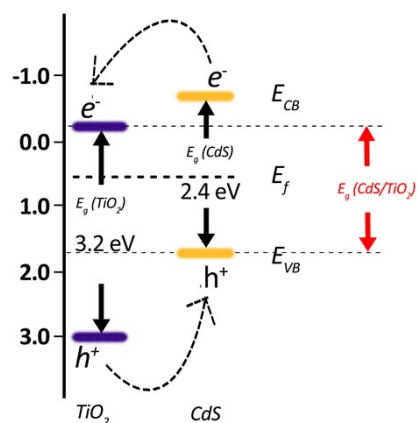


Fig.S9 Schematic diagram illustrating proposed band-edge structures and fermi level alignment for the electrodes of CdS/TiO₂.

As shown in Fig.S9, band gaps (E_g) of bare anatase TiO₂ and CdS are about 3.2 eV and 2.4 eV, respectively.^{6,7} Since the E_{CB} of CdS is more negative than that of TiO₂, a cascade energy level structure is formed via the combination of CdS and TiO₂. Therefore, the E_g of CdS/TiO₂ heterojunction structure is narrower than either E_g of CdS or E_g of TiO₂. Moreover, the favorable alignment of the fermi levels at CdS/TiO₂ interfaces facilitates electron injection and hole recovery.

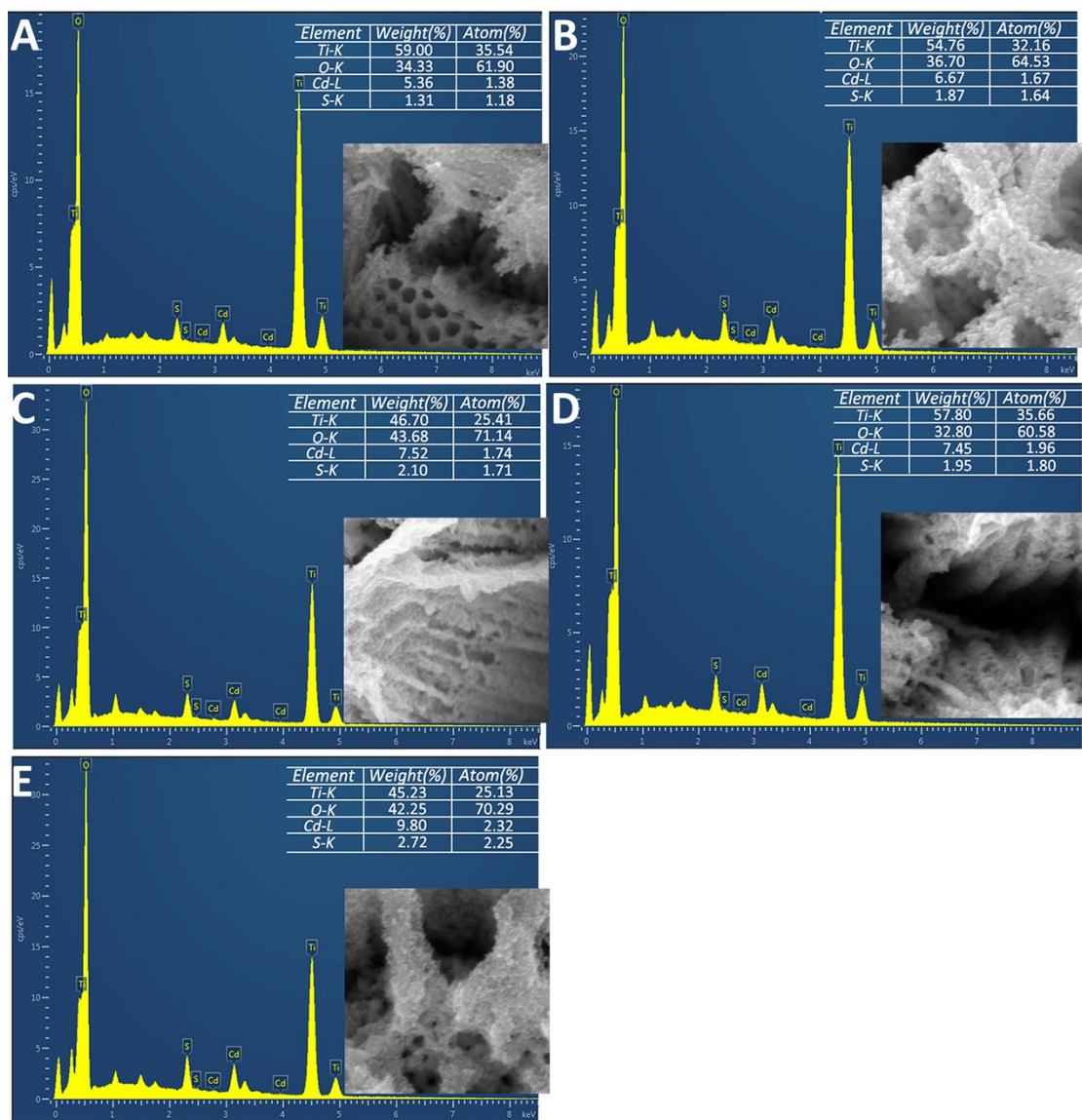


Fig.S10 SEM images (the inserts) and EDS patterns of CdS/TiO₂ WTs (A), CdS/TiO₂ PWTs (B), CdS/TiO₂FWTs (C), CdS/TiO₂C₀₀₁WTs (D) and CdS/TiO₂C₁₁₁WTs (E) photoelectrodes.

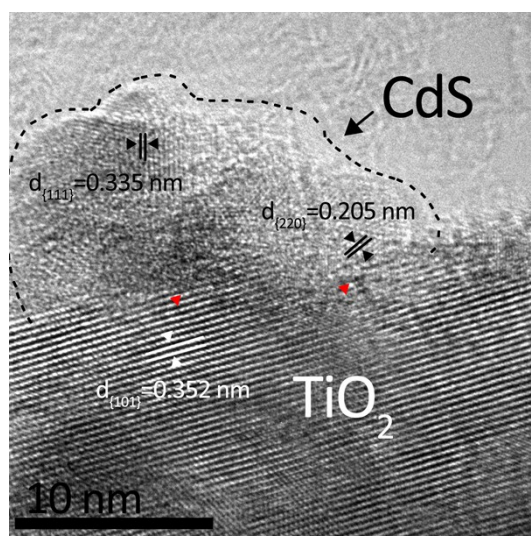


Fig.S11 High-resolution TEM (HR-TEM) image of CdS/TiO₂.

As shown in Fig.S11, lattice fringes with interplanar spacings $d_{\{111\}} = 0.335$ nm and $d_{\{220\}} = 0.205$ nm are consistent with the cubic phase of CdS [JCPDS no. 80-0019]. While $d_{\{101\}} = 0.352$ nm is correspond to the antase phase of TiO₂ [JCPDS no. 71-1166]. The $\{220\}$ planes of CdS are connected to the $\{101\}$ planes of TiO₂ with certain angles (interfaces between CdS and TiO₂ where red arrows exist), indicating that CdS QDs are grown on the TiO₂. Compared with the simple adsorption interface, this growth interfaces (heterojunction) of CdS/TiO₂ could provide more charge transfer channels, which can enhance the electronic injection.

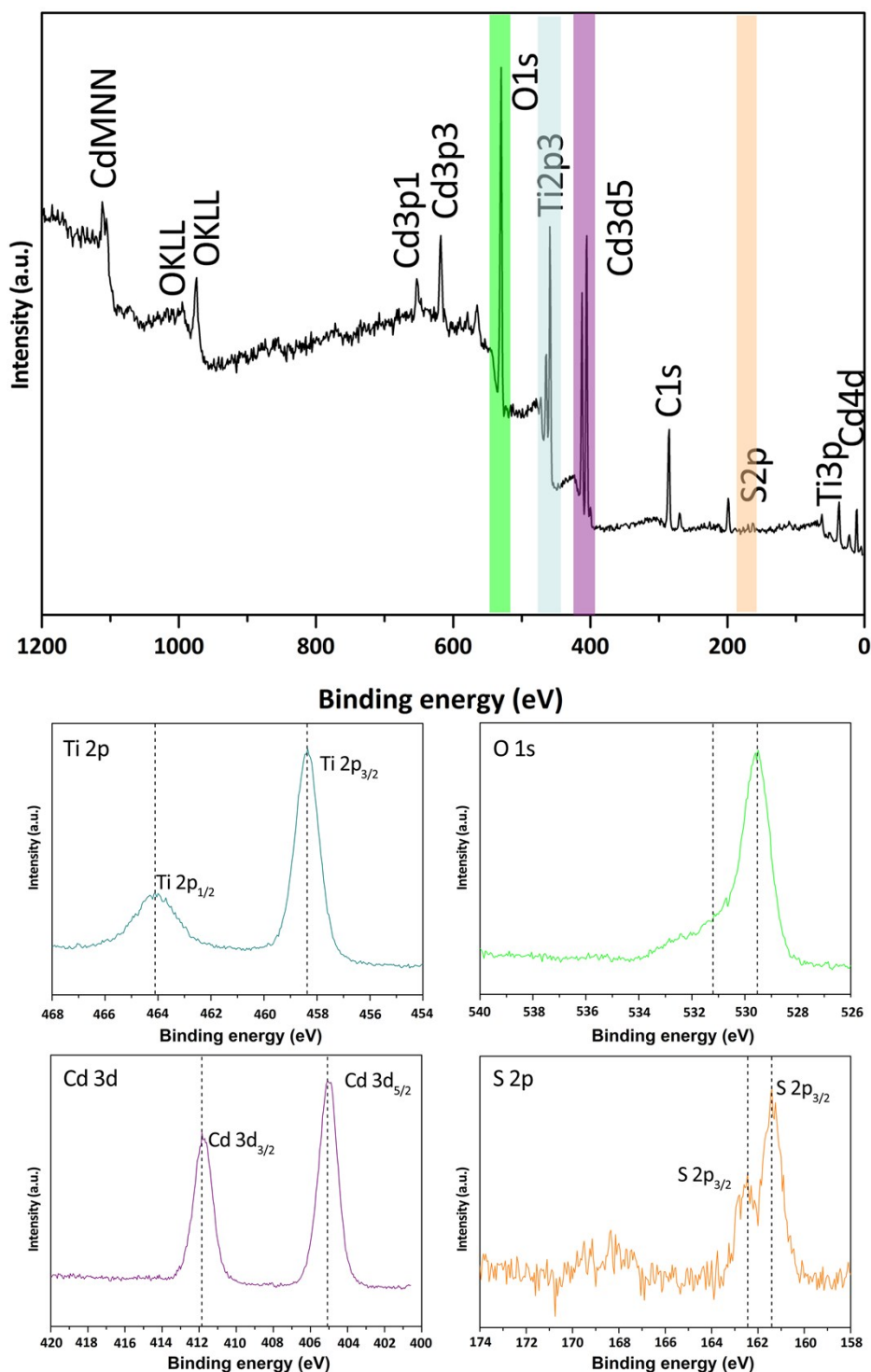


Fig.S12 XPS spectra of CdS/TiO₂: survey XPS spectrum and high resolution spectra of Ti 2p, O 1s, Cd 3d and S 2p.

The characteristic peaks of Ti 2p, O 1s, Cd 3p, Cd 3d, S 2p and C 1s can be clearly identified. The C element can be attributed to the trace hydrocarbon from the XPS instrument itself. Strong peaks at 458.4 eV and 464.1 eV in high-resolution XPS spectra of the Ti element are assigned to Ti⁴⁺ 2p_{3/2} and Ti⁴⁺ 2p_{1/2}, respectively. In

high-resolution XPS spectra of the O element, the strong peak at 529.8 eV and the small peak at 531.4 eV can be assigned to the anionic oxygen in the TiO₂ lattice and the oxygen in a surface hydroxyl, respectively. Strong peaks at 411.8 eV and 405.1 eV are assigned to Cd²⁺ 3d_{3/2} and Cd²⁺ 3d_{5/2}, respectively. However, the binding energy of S2p_{3/2} was located at 162.8eV and 161.8eV, respectively. The 1eV difference between the binding energies of S2p_{3/2} peaks was characteristic of S²⁻ states, i.e. Ti-S bond and Cd-S bond. It indicates that CdS are grown on TiO₂ by S bonding.

Table 1. ICP-AES performed by IRIS Advantage 1000 (Thermo Jarrell Ash Co.) was to characterize the concentration of Cd²⁺. CdS amounts for the samples were calculated from Cd and S with 1:1 stoichiometry.

| Samples | CdS amount (mg/cm ²) ^a |
|-------------------------------------------|-----------------------------------------------|
| CdS/TiO ₂ WTs | 9.91×10 ⁻³ |
| CdS/TiO ₂ PWTs | 25.66×10 ⁻³ |
| CdS/TiO ₂ FWTs | 36.12×10 ⁻³ |
| CdS/TiO ₂ C ₀₀₁ WTs | 55.17×10 ⁻³ |
| CdS/TiO ₂ C ₁₁₁ WTs | 66.77×10 ⁻³ |

^a CdS amount per unit area (mg/cm²)

Both the EDS and ICP-AES results show that TiO₂C₁₁₁WTs photoelectrode adsorbs more CdS QDs than other photoelectrodes.

References

- (1) H Xu, P Reunchan, S X Ouyang, H Tong, N Umezawa, T Kako and J H Ye, Anatase TiO₂ Single Crystals Exposed with High-Reactive {111} Facets Toward Efficient H₂ Evolution. *Chem. Mater.*, **2013**, 25, 405-411.
- (2) Gregorio F Ortiz, Ilie Hanzu, Philippe Knauth, Pedro Lavela, José L. Tirado, Thierry Djenizian, TiO₂ Nanotubes Manufactured by Anodization of Ti Thin Films for On-chip Li-ion 2D Microbatteries. *Electrochimica Acta*, **2009**, 54,4262–4268.
- (3) Khan, S. U.; Al-Shahry, M.; Ingler, W. B. Efficient Photochemical Water Splitting by a Chemically Modified n-TiO₂. *Science*, **2002**, 297, 2243–2245.
- (4) K. Darowicki, S. Krakowiak and P. Ślepski, Selection of measurement frequency in Mott–Schottky analysis of passive layer on nickel. *Electrochim. Acta*, **2006**, 51, 2204.
- (5) L. Zeiri, I. Patla, S. Acharya, Y. Golan, and S. Efrima, Raman Spectroscopy of Ultranarrow CdS Nanostructures. *J. Phys. Chem. C.*, **2007**, 111, 11843-11848.
- (6) R. Ashai, T. Morokawa, T. Ohwaki and Y. Taga, Visible-Light Photocatalysis in Nitrogen-Doped Titanium Oxides, *Science*, **2001**, 293, 269.
- (7) C. H. Chang and Y. L. Lee, Chemical bath deposition of CdS quantum dots onto mesoscopic TiO₂ films for application in quantum-dot-sensitized solar cells, *Appl. Phys. Lett.*, **2007**, 91, 053503.